

Microwave loss and intermodulation in $Tl_2Ba_2CaCu_2O_y$ thin films

Balam A. Willemsen

Superconductor Technologies, Inc., Santa Barbara, California 93111-2310

K. E. Kihlstrom

Superconductor Technologies, Inc., Santa Barbara, California 93111-2310
and *Department of Physics, Westmont College, Santa Barbara, California 93108-1099*

T. Dahm and D. J. Scalapino

Department of Physics, University of California, Santa Barbara, California 93106-9530

B. Gowe, D. A. Bonn, and W. N. Hardy

Department of Physics and Astronomy, University of British Columbia, Vancouver, British Columbia, Canada

(Received 8 April 1998)

A superconducting microstrip hairpin resonator is used as a tool to study the linear and nonlinear microwave response of TBCCO thin films. We extract the surface resistance $R_s(T)$, penetration depth $\lambda(T)$, and intermodulation critical current $J_{\text{IMD}}(T)$ for such a resonator at 4.2 GHz. The surface impedance results compare well with cavity perturbation measurements on portions of the same wafer. $J_{\text{IMD}}(T)$ is compared against theoretical models for the intrinsic nonlinear response of s - and d -wave superconductors. We demonstrate that the dc critical current J_c and J_{IMD} are distinct material parameters, describing different physical regimes. [S0163-1829(98)06734-4]

I. INTRODUCTION

The low microwave surface resistance of high- T_c superconducting (HTS) thin films at liquid-nitrogen temperatures allows for small, low-loss resonators, and thus highly selective filters, to be fabricated. However, the high current densities that arise due to the size and thin-film nature of these structures lead to nonlinear effects at relatively modest power levels, which are undesirable for most applications. These nonlinear microwave effects, such as intermodulation and harmonic generation, have been the subject of a flurry of recent theoretical and experimental work in both HTS resonators and filters.^{1-7,11}

Thallium cuprates are particularly attractive for applications since they have transition temperatures in excess of 100 K, or about 10–15 K higher than $YBa_2Cu_3O_{7-\delta}$. The higher transition temperatures allow for devices to be operated at lower reduced temperatures where the superconducting properties are better established.

Here, we use a hairpin resonator (as shown in Fig. 1) to study the linear and nonlinear microwave response of superconducting $Tl_2Ba_2CaCu_2O_y$ (TBCCO) thin films. This structure is slightly more complex than a simple straight half wave resonator, since the currents in the two legs of the resonator interact. However, it remains far less complex than a typical quasilumped element resonator or filter. We previously studied the dependence of the losses and the intermodulation power on the geometry of this resonator, particularly the size of the gap between its two legs, and measured the performance of the device in its fundamental and first harmonic modes.⁸ We introduced the intermodulation critical current J_{IMD} as a material parameter, characterizing the nonlinear intermodulation response independent of the device

properties.⁷ In the present work we want to focus on the temperature dependence of the quality factor, resonance frequency, and intermodulation power from which we can extract surface resistance, penetration depth, and intermodulation critical current as a function of temperature. We compare the temperature dependence of J_{IMD} with different microscopic models, which allows us to gain some insight into the microscopic origin of the nonlinear effects in our films and gives us a parameter for nonlinear film characterization.

In order to relate measured device properties to material properties, we must perform precise numerical calculations for a system composed of two coupled superconducting microstrip lines. In these calculations we use the quasi-TEM method of Weeks *et al.*⁹ and Sheen *et al.*¹⁰ to calculate the current distribution in the legs of the resonator from which we determine the quality factor and intermodulation power (for more details, see Refs. 7 and 11). This treatment neglects the bend of the hairpin resonator.

II. MATERIAL CHARACTERIZATION

Superconducting TBCCO was deposited on both sides of a 2 in.-diam, 0.38 mm-thick MgO substrate using our stan-

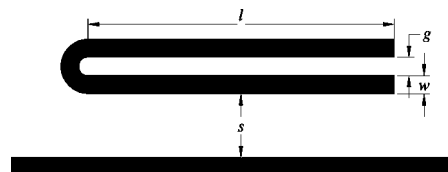


FIG. 1. Geometry of the hairpin resonator studied in this work. The two legs of the resonator with length l and linewidth w are separated by a gap distance g . The coupling of the resonator to the transmission line is adjusted by the separation s .

dard process.¹² The resulting films were approximately 6000 Å thick and had a nominal T_c of 100.0 ± 0.5 K as measured by ac susceptibility at several points across the wafer. The microwave circuits were patterned on one side of the wafer using standard photolithography and then the wafer was diced into individual 6×10 mm² chips.

Portions of the wafer were reserved for material characterization and other experiments. The surface resistance of a 4 mm-diameter disc patterned from the same wafer measured at 77 K and 3.7 GHz at the University of British Columbia (UBC) was $R_s = 53 \mu\Omega$. Using ω^2 scaling this would correspond to $380 \mu\Omega$ at 10 GHz or $68 \mu\Omega$ at 4.2 GHz.

The 3.7 GHz measurements were performed using a cavity perturbation technique. The microwave cavity, which is described in detail elsewhere,¹³ is a superconducting splitting resonator developed for high-sensitivity measurements of small, low-loss samples. The 4 mm-diam. TBCCO disc was mounted on a temperature controlled sapphire finger and measurements of the surface resistance were performed by comparing the Q of the unloaded split-ring resonator to the Q when the disc was inserted into the rf microwave magnetic fields of the resonator. The accuracy of the technique is estimated to be better than $\pm 5 \mu\Omega$ for a 4 mm-diam sample being measured at 3.7 GHz.

III. BAND REJECT HAIRPIN RESONATORS

The geometry of a hairpin resonator (see Fig. 1) is determined by three parameters: the linewidth w , length l , and the gap between the two legs of the resonator, g . Microwave energy is coupled to a resonator in a band reject fashion by placing it parallel to a 50Ω transmission line. The spacing s , between the transmission line and the resonator, determines the strength of the coupling and thus the energy stored in the resonator, which can be characterized in terms of the loaded quality factor Q_L of the device.

The response of a band reject resonator can be characterized in terms of three quantities, the resonance frequency f_0 , and the loaded and unloaded quality factors, Q_L and Q_U . f_0 and Q_L are determined by the geometry of the resonator and substrate and can be predicted using commercially available microwave design tools.

The resonator studied here had $w = 0.4$ mm, $g = 0.4$ mm, $s = 0.75$ mm, and $l = 6.77$ mm. It had a fundamental resonance at 4.2 GHz with Q_U in the tens of thousands and $Q_L = 1140$. The second resonance (at 7.4 GHz) was the subject of discussion elsewhere.⁸

The circuit was clipped into gold plated test fixtures. The microwave circuit was then completed by wire bonds at both ends of the 50Ω through line. The electrical ground plane for the resonator is primarily provided for by the unpatterned film on the back side of the substrate.

The temperature dependence of Q_U and the intermodulation products were measured under vacuum in a system using a CTI Cryogenics Model 22 refrigerator that provided temperatures down to near 20 K. A silicon diode thermometer was attached to the test fixture. We used a Lake Shore Model DRC-91C temperature controller to provide thermal stability (typically within ± 0.1 K) during the measurements.

The microwave transmission S_{21} was measured using a Hewlett/Packard HP8720B vector network analyzer in order

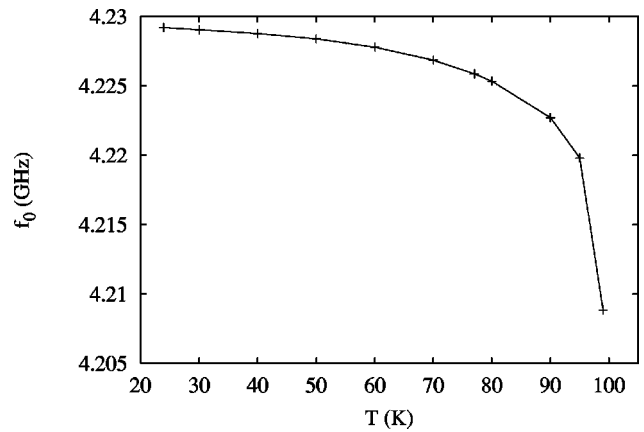


FIG. 2. Measured temperature dependence of the fundamental resonance frequency f_0 .

to determine f_0 and Q 's that characterize the linear response of the circuit at low microwave powers. The Q 's are obtained from direct measurements of the width of the resonance 3 dB above the minimum, $\Delta f_{+3 \text{ dB}}$. The input power (P_{IN}) for the resonators was varied from -10 to -40 dBm. Data was taken between 23 K and T_c with a higher density of points at higher temperatures.

Figure 2 shows f_0 as a function of temperature. The change in frequency is fairly small until the temperature approaches T_c , where it drops much more rapidly. Figure 3 shows Q versus T , where again most of the change occurs near T_c , although Q continues to rise as the temperature drops.

The two microwave signals required to produce intermodulation products were symmetrically placed 15 kHz above and below f_0 , for a signal separation of 30 kHz. Continuous wave signals were produced using HP8341B and HP83640A synthesized sweepers, and the signals detected using a Tektronix 2784 spectrum analyzer. The output power of the two sources was measured using an HP 437B power meter, and adjusted so that the two signals arrived at the sample with the same magnitude.

We then measured the absolute magnitude of the third-order intermodulation products, $P_{\text{IMD}} (= P_{2\omega_1 - \omega_2} = P_{2\omega_2 - \omega_1})$, as a function of $P_{\text{IN}} (= P_{\omega_1} = P_{\omega_2})$, input

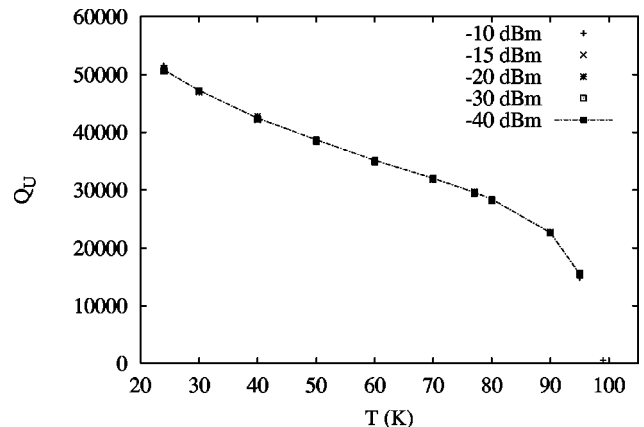


FIG. 3. Measured temperature dependence of the unloaded quality factor Q_U in the fundamental resonance. Note that Q_U is power independent up to the highest power level studied here.

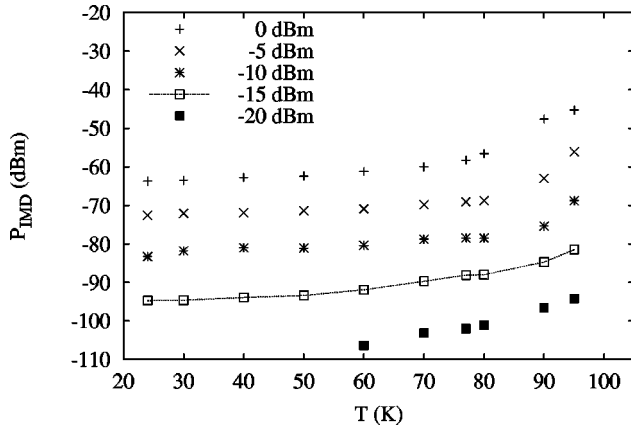


FIG. 4. The intermodulation power $P_{\text{IMD}}(T)$ presented for various input power levels. Note the relatively flat temperature dependence at low T .

power provided to the device and temperature (again from 23 K to near T_c). For the 30 kHz signal separation we are using here, these signals are generated at $f_0 \pm 45$ kHz. The results for the lower side band are shown in Figure 4. Below 70 K there is not much change, but again as the temperature approaches T_c , there is some degradation. The results for the upper side band were very similar. Below 60 K the measured values fall below our -110 dBm noise floor for the lowest input power, -20 dBm.

IV. EXTRACTION OF SURFACE IMPEDANCE AND PENETRATION DEPTH

We can use our numerical calculations to convert our measured $f_0(T)$ and $Q_U(T)$ into $R_s(T)$ and $\Delta\lambda(T)$. We follow the method of Oates, Anderson, and Mankiewich,^{10,14} but include the effects of coupling between the two legs of the hairpin resonator in our calculations of the inductance $L(\lambda)$ as indicated above (see also Ref. 11). For a given value of $\lambda(0)$, we can then find $\lambda(T)$ by comparing the numerical $L(\lambda)/L[\lambda(0)]$ with the experimentally determined

$$\frac{f_0^2(T=0)}{f_0^2(T)} = \frac{L(T)}{L(T=0)}. \quad (1)$$

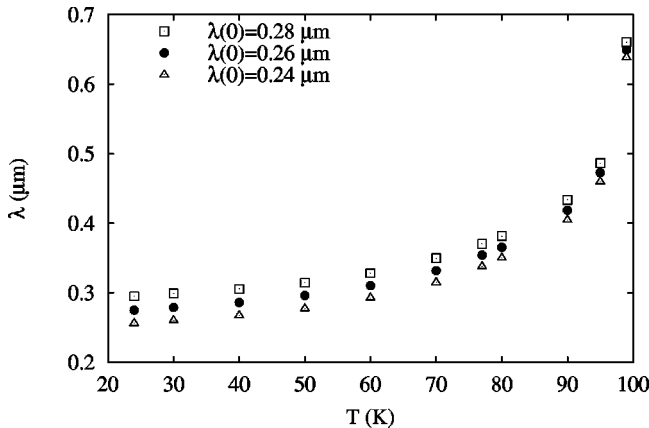


FIG. 5. The extracted temperature dependence of the penetration depth $\lambda(T)$ for various values of $\lambda(0)$.

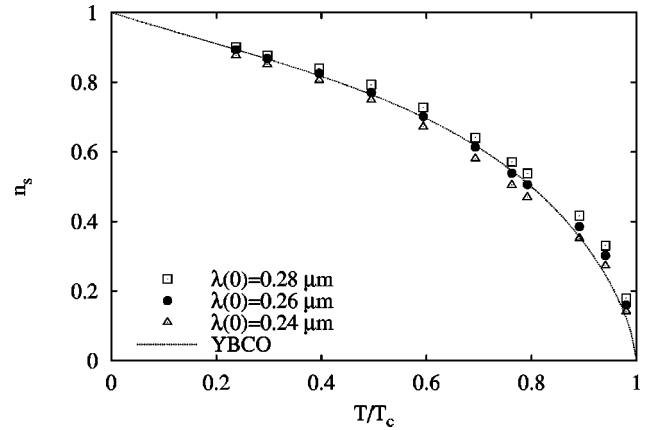


FIG. 6. $[\lambda(0)/\lambda(T)]^2$ for various values of $\lambda(0)$ as a function of T/T_c . The solid line is single-crystal YBCO data from Refs. 15 and 16.

In Fig. 5 we present the extracted $\lambda(T)$ for three different values of $\lambda(0)$.

In order to estimate $\lambda(0)$, we compare our penetration depth results with those from YBCO single crystals at UBC. Figure 6 shows $[\lambda(0)/\lambda(T)]^2$ for three different values of $\lambda(0)$ along with the YBCO a -axis data.^{15,16} We find that $\lambda(0)=0.26$ μm gives the best agreement. Note that this value is slightly bigger than our previous estimate of 0.3 μm at 77 K, which corresponds to $\lambda(0)=0.22$ μm .⁸

The values of λ thus generated are then used to convert our measured Q_U into a surface resistance R_s . Comparing the measured $Q_U(T)$ with the calculated $Q[\lambda(T), \sigma_1]$ yields the real part of the conductivity $\sigma_1(T)$. From this, we find R_s from

$$R_s(T) = 2\pi^2 \mu_0^2 f_0^2 \lambda^3(T) \sigma_1(T). \quad (2)$$

In Fig. 7 we show $R_s(T)$ thus obtained for the same values of $\lambda(0)$ as above.

The agreement between the 4.2 GHz microstrip data and the 3.7 GHz split-ring measurements is excellent below 60 K, providing a high degree of confidence in the geometric factors calculated to convert our microstrip Q s to R_s . The

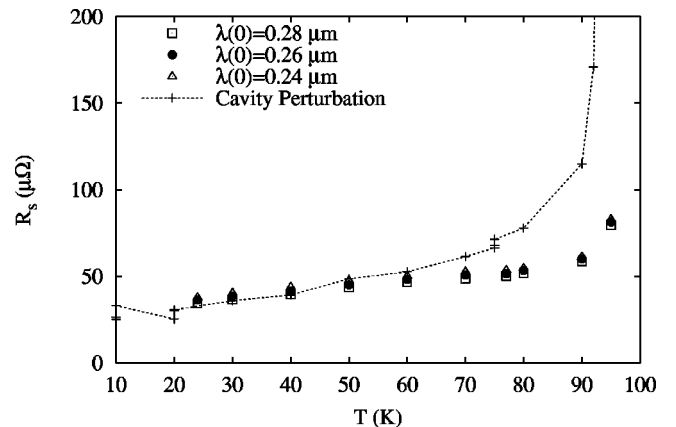


FIG. 7. The extracted surface resistance $R_s(T)$ for various values of $\lambda(0)$. The dashed line is data obtained using the cavity perturbation method and has been scaled from 3.7 to 4.2 GHz for comparison.

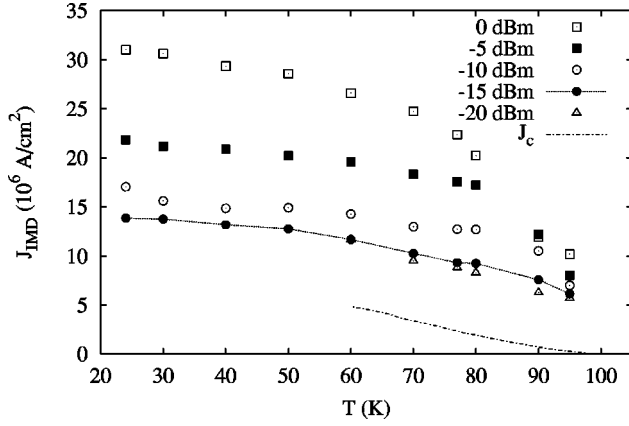


FIG. 8. The extracted intermodulation critical current $J_{\text{IMD}}(T)$. Note the relatively flat temperature dependence at low T . The dashed line shows the measured dc critical current $J_c(T)$.

deviation between the two data sets would seem to indicate that the T_c of the 4 mm disc is reduced by up to 10 K. The disc was patterned from a region of the film that is roughly 5 mm from the edge of the wafer to the center of the disc, film quality is typically lower here than in the bulk of the film due to variations in composition and oxygenation.

V. MICROWAVE INTERMODULATION CRITICAL CURRENT, J_{IMD}

In Refs. 7 and 8 we introduced the intermodulation critical current J_{IMD} as a material parameter to characterize the nonlinear intermodulation response at low power levels for a uniform superconductor. J_{IMD} serves as an expansion parameter for the lowest-order dependence of the penetration depth λ on the current density J :

$$\left(\frac{\lambda(0)}{\lambda(T, J)}\right)^2 = \left(\frac{\lambda(0)}{\lambda(T, J=0)}\right)^2 \left[1 - \left(\frac{J}{J_{\text{IMD}}(T)}\right)^2\right]. \quad (3)$$

From this we were able to calculate the intermodulation power for different microstrip geometries.^{7,8,11} (Note that we changed the notation slightly compared to Refs. 7 and 11).

We extract J_{IMD} from the measured intermodulation power P_{IMD} by comparing it with the calculated intermodulation power at a given power level and J_{IMD} , using the fact that P_{IMD} scales as J_{IMD}^{-4} . $J_{\text{IMD}}(T)$ is shown in Fig. 8. At low temperatures J_{IMD} shows a very flat temperature dependence.

It is instructive to compare these results with different models for the microscopic origin of the nonlinear behavior. In Ref. 7 the intrinsic nonlinearities of s - and d -wave superconductors were discussed. In Fig. 9 the temperature dependences of J_{IMD} for these cases are shown as the dashed and dotted lines, respectively. For a pure s -wave superconductor, nonlinear behavior disappears exponentially at low temperatures and thus $J_{\text{IMD}}(T)$ diverges. For a d -wave superconductor, on the other hand, nonlinear behavior should go through a minimum and become stronger at lower temperatures due to the nodes in the gap function, as has been discussed by Xu, Yip, and Sauls¹⁷ and in Ref. 7. Thus J_{IMD} should become smaller. As a simple model for weak links, we show the behavior one would expect for a series of Jo-

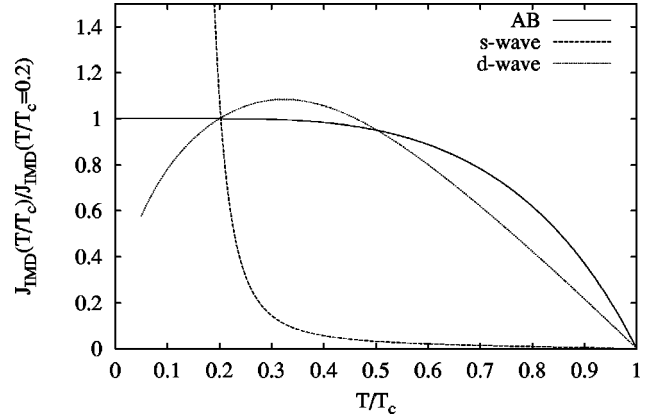


FIG. 9. The temperature dependence of J_{IMD} for the three different models described in Sec. V (solid line: JJ model, dotted line: intrinsic d wave, dashed line: intrinsic s wave). The current density is normalized to the value at $T/T_c=0.2$ in each case.

sephson junctions (JJ) in the legs of the resonator. In this case, J_{IMD} follows the Ambegaokar-Baratoff form^{18,19}

$$\frac{J_{\text{IMD}}(T)}{J_{\text{IMD}}(0)} = \frac{\Delta(T)}{\Delta(0)} \tanh\left(\frac{\Delta(T)}{2k_B T}\right). \quad (4)$$

Here we took the BCS temperature dependence for $\Delta(T)$ with $2\Delta(0)/k_B T_c = 6$, a typical value for high- T_c superconductors. Clearly, our results are closer to the JJ model, which is reasonable since the magnitude of J_{IMD} for pure s - and d -wave superconductors has been estimated to be of the order of $3 \cdot 10^8$ A/cm² (see Ref. 7) and thus much higher than our experimentally determined values. This suggests that weak links might dominate the nonlinear behavior at least at low power levels, but does not exclude the possibility that flux penetration might play an important role as well, once the magnetic fields at the edges of the legs reach the lower critical field H_{c1} .

Note that since the intermodulation products for TBCCO films do not usually scale like the third power of the input power, that the extracted J_{IMD} is power dependent. The low-power limit of this quantity can serve as a material parameter and gives us a characteristic current density for the intermodulation distortion. Our data clearly shows that J_{IMD} becomes smaller with decreasing input power. We therefore estimate this low-power limit to be of the order of 10^7 A/cm² at low temperatures. P_{IMD} appears to have a $\sim 3:1$ slope at the lowest available powers above 60 K, where we still were able to detect P_{IMD} at $P_{\text{IN}} = -20$ dBm. This means that, in this region, the values of J_{IMD} for the two lowest powers agree, lending further weight to our argument that the low-power limit is a close upper bound to the zero-power limit.

In Fig. 8 we also show measurements of the dc critical current $J_c(T)$ on the same wafer. The superconducting material was patterned into a configuration for four-point resistance measurements. The width of the measured section is 20 μm and its length is 600 μm . Temperature control was provided using the same system described above for the resonator measurements. We use both a leader LFG-1300S function generator (currents of up to roughly 100 mA) and an HP 6294A dc power supply (currents from 100 mA up to 800

mA) to provide current for the measurements. A 49.9 Ω sensing resistor was used to measure the current accurately. Both the junction voltage and sensing voltage were displayed on a Tektronix 7603 oscilloscope. The critical current is determined by increasing the current to the sample until the onset of junction voltage (typically detectable at about 2 μ V). Dividing this current by the cross-sectional area gives J_c . Four distinct J_c bridges were available close to the position of the resonator on the wafer, the J_c variation over these 4 samples was of the order of 10%.²⁰

As can immediately be seen from Fig. 8, J_c and J_{IMD} have significantly different temperature dependences although the two quantities are similar in magnitude. While the dc critical current increases from $J_c = 2.4 \times 10^6$ A/cm² at $T = 77$ K to $J_c = 4.8 \times 10^6$ A/cm² at $T = 60$ K, J_{IMD} has only increased by 33% from 8.8 to 11.7×10^6 A/cm². These two different characteristic current densities are not necessarily connected with each other. While J_{IMD} describes the low-power, microwave behavior of the material, J_c characterizes the high-power, dc behavior.

Recently, Takken, Beasley, and Pease²¹ measured the rf breakdown critical current density $J_{c,\text{RF}}$ for YBCO and compared this to the DC transport critical current J_c . It was found that $J_{c,\text{RF}}$ is usually much smaller than J_c . It was also suggested that $J_{c,\text{RF}}$ might be improved by better edge quality of the film, and that the rf power handling capability of the films would then also improve. We want to emphasize that this would not necessarily lead to an improvement of intermodulation products, P_{IMD} . Particularly, certain types of edge defect (Ref. 11) lead to a dramatic suppression Q (and thus power handling), while having limited impact on P_{IMD} . The effects that are discussed in this paper occur at power levels that are many orders of magnitude below the sort of rf breakdown effects discussed by Takken can be observed, and thus it should not be surprising that they are governed by different physical parameters. Thus, if one seeks

a reduction of nonlinear response in this low-power regime, J_{IMD} is the more appropriate parameter for optimization and discussion.

VI. CONCLUSIONS

Measuring the device properties of a high- T_c superconducting microstrip hairpin resonator, we were able to extract the temperature dependence of the surface resistance, the penetration depth, and the intermodulation critical current of $\text{Ti}_2\text{Ba}_2\text{CaCu}_2\text{O}_y$ thin films. For a penetration depth of $\lambda(0) = 0.26$ μm the temperature dependence of $[\lambda(0)/\lambda(T)]^2$ is in good agreement with previous YBCO single-crystal data, as has been found earlier.²² The intermodulation critical current J_{IMD} has a relatively flat temperature dependence at low temperatures similar to what one would expect from weak links and unlike the behavior expected for the intrinsic nonlinear response of *s*- or *d*-wave superconductors. This temperature dependence is different than the one for the dc critical current J_c and shows that these two quantities describe different regimes of the nonlinear behavior, J_{IMD} characterizing the low-power, microwave response and J_c the high-power, dc response. For a characterization of the intermodulation distortion from a high- T_c film below rf breakdown, J_{IMD} is the more appropriate material parameter.

ACKNOWLEDGMENTS

We would like to thank S. Jimenez, V. Cisneros, and J. Mitchell for their technical assistance, as well as A. Cardona, M. M. Eddy, N. O. Fenzi, R. B. Hammond, G. L. Matthaei, and J. R. Schrieffer for invaluable discussions related to this problem. T.D. would like to acknowledge the hospitality of the UCSB Physics Department and support of the Deutsche Forschungsgemeinschaft, as well as support from Superconductor Technologies Inc. D.J.S. acknowledges support from the NSF under Grant No. DMR 95-27304.

- ¹G.-C. Liang, D. Zhang, C.-F. Shih, M. E. Johanson, R. S. Withers, D. E. Oates, A. C. Anderson, P. Polakos, P. M. Mankiewich, E. de Obaldia, and R. E. Miller, *IEEE Trans. Microwave Theory Tech.* **43**, 3020 (1995).
- ²C. Wilker, Z.-Y. Shen, P. Pang, W. L. Holstein, and D. W. Face, *IEEE Trans. Appl. Supercond.* **5**, 1665 (1995).
- ³Z. Ma, E. de Obaldia, G. Hampel, P. Polakos, P. Mankiewich, B. Batlogg, W. Prusseit, H. Kinder, A. Anderson, D. E. Oates, R. Ono, and J. Beall, *IEEE Trans. Appl. Supercond.* **7**, 1911 (1997).
- ⁴G. Hampel, B. Batlogg, K. Krishana, N. P. Ong, W. Prusseit, H. Kinder, and A. C. Anderson, *Appl. Phys. Lett.* **71**, 3904 (1997).
- ⁵J. McDonald, J. R. Clem, and D. E. Oates, *Phys. Rev. B* **55**, 11 823 (1997); *J. Appl. Phys.* **83**, 5307 (1998).
- ⁶W. Diete, M. Getta, M. Hein, T. Kaiser, G. Müller, H. Piel, and H. Schlick, *IEEE Trans. Appl. Supercond.* **7**, 1236 (1997).
- ⁷T. Dahm and D. J. Scalapino, *Appl. Phys. Lett.* **69**, 4248 (1996); *J. Appl. Phys.* **81**, 2002 (1997).
- ⁸B. A. Willemsen, T. Dahm, and D. J. Scalapino, *Appl. Phys. Lett.* **71**, 3898 (1997).
- ⁹W. T. Weeks, L. L. Wu, M. F. McAllister, and A. Singh, *IBM J. Res. Dev.* **23**, 652 (1979).
- ¹⁰D. M. Sheen, S. M. Ali, D. E. Oates, R. S. Withers, and J. A. Kong, *IEEE Trans. Appl. Supercond.* **1**, 108 (1991).
- ¹¹T. Dahm and D. J. Scalapino, *J. Appl. Phys.* **82**, 464 (1997).
- ¹²M. M. Eddy, U.S. Patent 5,476,836 (1995); 5,508,255 (1996).
- ¹³D. A. Bonn, D. C. Morgan, and W. N. Hardy, *Rev. Sci. Instrum.* **62**, 1819 (1991).
- ¹⁴D. E. Oates, A. C. Anderson, and P. M. Mankiewich, *J. Supercond.* **3**, 251 (1990).
- ¹⁵D. A. Bonn, S. Kamal, K. Zhang, R. Liang, and W. N. Hardy, *J. Phys. Chem. Solids* **56**, 1941 (1995).
- ¹⁶D. A. Bonn and W. N. Hardy, in *Physical Properties of High Temperature Superconductors V*, edited by D. M. Ginsberg (World Scientific, Singapore, 1996).
- ¹⁷S. K. Yip and J. A. Sauls, *Phys. Rev. Lett.* **69**, 2264 (1992); D. Xu, S. K. Yip, and J. A. Sauls, *Phys. Rev. B* **51**, 16 233 (1995).
- ¹⁸V. Ambegaokar and A. Baratoff, *Phys. Rev. Lett.* **10**, 486 (1963).
- ¹⁹M. Tinkham, *Introduction to Superconductivity*, 2nd ed. (McGraw-Hill, New York, 1996).
- ²⁰The normal-state resistivity of the sample from these measurements was found to be $\rho(110\text{ K}) \sim 90$ $\mu\Omega$ cm.
- ²¹T. E. Takken, M. R. Beasley, and R. F. W. Pease (unpublished); T. E. Takken, Ph.D. thesis, Stanford University, 1997.
- ²²Z. Ma, Ph.D. thesis, Stanford University, 1995.